ELSEVIER

Earth and Planetary Science Letters 151 (1997) 117–123

EPSL

Express Letter

The Mid-Pleistocene climate transition: onset of 100 ka cycle lags ice volume build-up by 280 ka

Manfred Mudelsee [a,1], Michael Schulz [b,*]

[a] *Geologisch–Paläontologisches Institut, Universität Kiel, Olshausenstrasse 40, D-24118 Kiel, Germany*
[b] *Sonderforschungsbereich 313, Universität Kiel, Heinrich-Hecht-Platz 10, D-24118 Kiel, Germany*

Received 5 April 1997; accepted 19 June 1997

Abstract

The Mid-Pleistocene Climate Transition (MPT) is the complex climatic change which brought the Late Pleistocene ice ages. We explore the MPT in the time and frequency domains by new methods of time series analysis. High-resolution oxygen isotope records reveal that the ice volume-related increase in δ^{18}O mean (amplitude: 0.29 ± 0.05 $(1 - \sigma_\mu)$ ‰, transition midpoint: 922 ± 12 ka, duration: 40 ± 9 ka) significantly preceded the abrupt increase in the amplitude of the $\sim$ 100 ka cycle at 641 ± 9 ka. This finding can be quantitatively simulated using a simple ice–bedrock model in which, due to the additional ice, the calving threshold is exceeded. The simulated calving events prior to $\sim$ 650 ka are separated by $\sim$ 77 ka, whereas after $\sim$ 650 ka they occur pseudo-periodically with a mean period of nearly 100 ka. The cause for the delay of the $\sim$ 100 ka calving cycle was not a slow bedrock relaxation; rather, the coincidental combination of insolation, existing ice mass, and bedrock depression. © 1997 Elsevier Science B.V.

Keywords: Pleistocene; marine sediments; O-18/O-16; climate; glaciation; time series analysis; models

1. Introduction

The Mid-Pleistocene Climate Transition (MPT) led to the Late Pleistocene ice ages. High-resolution and precision-dated marine oxygen isotope (δ^{18}O) records have become available, which document the history of continental ice volume across the MPT (see Table 1). A precise knowledge of the transitional behaviour is essential for successful modelling (e.g. [1]) of Pleistocene climate evolution.

In the time domain, the MPT has been associated with an increase in time-dependent δ^{18}O mean lasting from 920 to 900 ka [2]. Prell [3] and Maasch [4] have previously reported an abrupt transition at about 900 ka, consisting of an ice volume-related δ^{18}O amplitude of ''somewhat less than'' 0.36‰ vs. PDB, or 0.18‰, respectively.

A second aspect of the MPT concerns changes in the frequency domain. Prior to the MPT, ice volume variations were dominated by the 41 ka cycle, whereas $\sim$ 100 ka periodicity has controlled climatic variability since then (e.g. [5]). According to Pisias

* Corresponding author. Fax: +49 431 880 1569. E-mail: mschulz@sfb313.uni-kiel.de
[1] Fax: +49 431 880 4376. E-mail: mam@zaphod.gpi.uni-kiel.de

PII S0012-821X(97)00114-3

Table 1
Foraminiferal $\delta^{18}O$ database

Core	Location	Habitat	Data	Timescale	Resolution [a]
DSDP 552	56°N, 23°W	benthic	[14]	untuned [b]	5.5 ka
DSDP 607	41°N, 33°W	benthic	[6]	tuned [c]	3.7 ka
ODP 659	18°N, 21°W	benthic	[15]	[15]	4.2 ka
ODP 677	01°N, 84°W	benthic	[16,17]	[17]	2.7 ka
ODP 806	00°N, 159°E	planktonic	[18]	[7]	4.0 ka

[a] Average value within the interval (250 ka; 1250 ka).
[b] Fixed points: core top, Brunhes/Matuyama = 769 ka, Jaramillo base = 1009 ka.
[c] After [17] (M. Raymo, pers. commun., 1994).

and Moore [5], this transition was abrupt at 900 ka. Ruddiman et al. [6] found that the 100 ka amplitude generally increased between 900 and 400 ka with the fastest changes occurring between 700 and 600 ka. This view was supported by Berger et al. [7] who referred to the 'Milankovitch chron' as the last 620 ka, where a strong 100 ka cycle occurred. Lau and Weng [8] concluded that the transition was abrupt at 700 ka. Park and Maasch [9] tended towards a gradual transition that took place between 1000 and 500 ka. Bolton et al. [10] favoured a multi-step transition starting at $\sim$ 900 ka and strongest at around 750 ka.

Here we differentiate (in a time versus frequency domain) and quantify the MPT precisely, using statistical methods of time series analysis developed by ourselves [11,12]. The supposed delay between the increase in mean ice volume and the subsequent increase in 100 ka amplitude is confirmed and its length determined. The observed transitional characteristics, including the delay, can be quantitatively simulated using an ice–bedrock model.

2. Statistical methods

In order to quantify the MPT in the *time domain*, the time-dependent $\delta^{18}O$ mean of the time series has to be estimated. For detecting a transition, optimal smoothing is performed using a rectangular window which has width H (running mean). The resulting noise reduction is, however, accompanied by a broadened transition ($\pm H/2$; Fig. 1); that is, a systematic error leading to an apparent longer duration. This trade-off problem can be solved by means of Monte-Carlo simulations by which the optimal window width is determined as a best compromise between systematic errors and noise [11].

For estimating the transition parameters (midpoint, duration and amplitude), a 'ramp function' (constant–linear–constant) is fitted to the original data (Fig. 1). Parameter errors are estimated using Monte-Carlo simulations: the standard deviation of the data is allowed to vary with time, resulting in a more realistic approach to modelling climate data.

In order to quantify the MPT in the *frequency domain*, the time-dependent amplitude (envelope) of the 100 ka signal component has to be estimated from the time series. Ferraz-Mello [13] devised an algorithm for harmonic filtering that can be adapted for this purpose.

The amplitude and phase of the sinusoidal filter function are estimated from the data by means of least-squares. In order to use this method for 100 ka envelope estimations, the time series are split into overlapping segments, using a sliding rectangular window as before. The estimated envelope has the same physical units as the original data. An advantage of this approach is that unevenly spaced time series can be processed directly. A window width of $H = 400$ ka offers a good compromise between statistical and systematic errors [11,12] and is therefore used for all analyses (Fig. 2).

3. Results

Fig. 1 shows the time-dependent means across the MPT for the $\delta^{18}O$ time series listed in Table 1. The measured $\delta^{18}O$ courses are covered by the $1-\sigma$

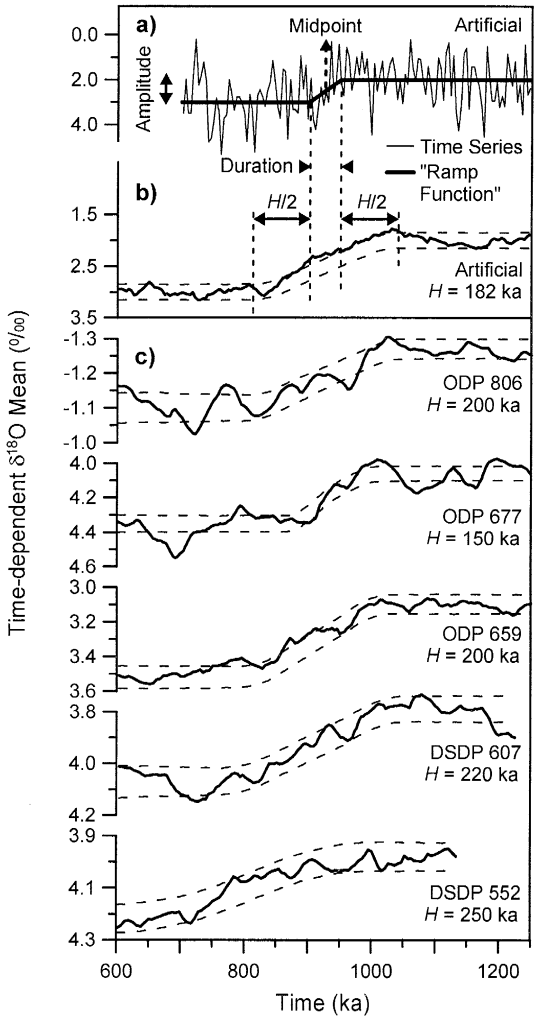

Fig. 1. Estimation of time-dependent mean. (a) The method is tested using an artificial time series which consists of a transition in mean and superimposed white noise. 'Ramp function' (heavy line) is used for estimating the transition parameters (midpoint, duration and amplitude). (b) Smoothed representation of the artificial time series, using a sliding rectangular window of optimal width H. The transition appears broadened by $\pm H/2$. The $1-\sigma$ standard error band of the best fit (dashed line) is calculated from 2500 Monte-Carlo simulations based on the (time-dependent) standard deviation. Estimated transition parameters coincide with the true values of the artificial time series. (c) As (b) but for the δ^{18}O data. The optimal window width is determined separately for each time series, depending on the duration and the signal-to-noise ratio of a transition, and the time resolution.

standard error bands of the best 'ramp function' fits. In case of the four high-resolution, astronomically tuned time series DSDP 607, ODP 659, ODP 677 and ODP 806, the estimated transition midpoints agree strikingly well (Table 2). The estimated durations and amplitudes agree reasonably well, reflecting minor local components. Averaging the estimated parameter values (Table 2) results in a midpoint of 922 ± 12 ka, a duration of 40 ± 9 ka, and a

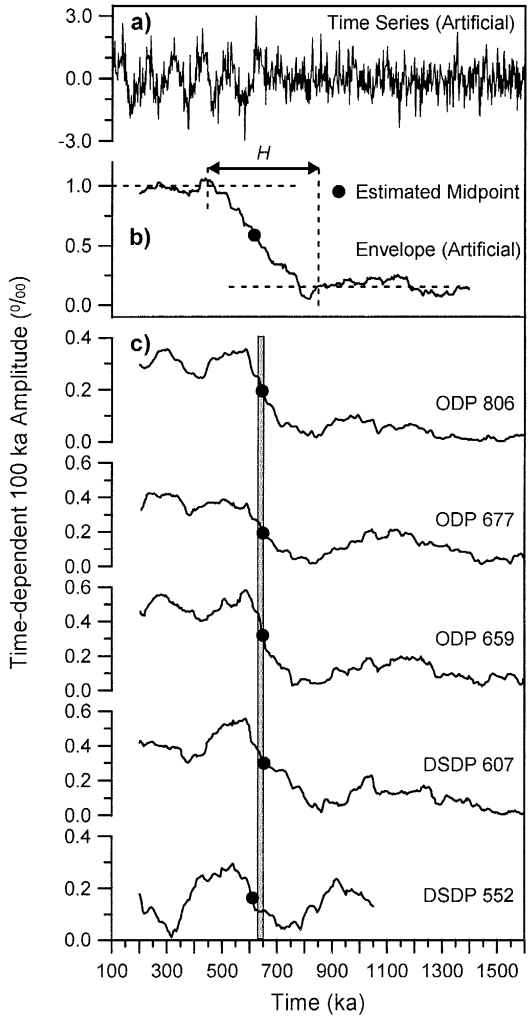

Fig. 2. Estimation of time-dependent 100 ka amplitude (envelope). (a) The method is tested using an artificial time series which consists of an abrupt transition in time-dependent 100 ka amplitude (at $T = 650$ ka, from 0.0 to 1.0‰) and superimposed white noise. (b) Due to the non-zero segment length ($H = 400$ ka), the estimated transition has an apparent duration of $\sim H$. Transition midpoint (average of pre- and post-transition amplitudes, horizontal dashed lines) and amplitude change across the transition are correctly estimated. (c) As (b) but for the δ^{18}O data. The shaded bar marks the average of the estimated midpoints.

Table 2
MPT characteristics of the $\delta^{18}O$ data

Core	T_{mean} (ka)	Δ (ka)	A (‰)	$T_{100\ ka}$ (ka)
DSDP 552	[810 ± 64]	[160 ± 20]	[0.24 ± 0.014]	607
DSDP 607	920 ± 35	70 ± 10	0.28 ± 0.014	651
ODP 659	915 ± 23	45 ± 5	0.42 ± 0.014	651
ODP 677	925 ± 17	18 ± 5	0.29 ± 0.014	650
ODP 806	925 ± 40	48 ± 5	0.17 ± 0.014	647
Average	922 ± 12	40 ± 9	0.29 ± 0.05	641 ± 9

Midpoint time (T_{mean}), duration (Δ) and amplitude (A) of the transition in the time domain. Midpoint time ($T_{100\ ka}$) of the transition in the frequency domain. Data in brackets have not been used for averaging (see text). Error quotations are $1-\sigma$ for data and $1-\sigma_{\mu}$ (maximum of internal/external error) for averages.

$\delta^{18}O$ amplitude of 0.29 ± 0.05‰. These averages corroborate the findings of the previous studies mentioned above and state them more precisely. The DSDP 552 time series exhibits a 'slow' $\delta^{18}O$ increase across the MPT, which differs significantly from the transitional behaviours of the other records (Table 2). The poorer time resolution, a possibly inaccurate timescale, or the inadequacy of the assumed 'ramp transition' may account for this. Therefore, the result from this time series has been excluded from calculation of the averages of the transition parameters.

Fig. 2 shows the estimated 100 ka envelopes across the MPT. In all cases the estimated transition has an apparent duration of ≤ 400 ka (i.e., $\leq$ the window width H) and is thus consistent with an abrupt amplitude change. The transition midpoints (Table 2) coincide fairly well with an average of 641 ± 9 ka. This value and the detected abruptness are also compatible with some findings mentioned above. The corresponding 41 ka envelopes ([11]; not shown) do not exhibit significant variations across the MPT.

The accuracy of the 100 ka envelope estimates is regarded as high since the age models of the $\delta^{18}O$ records used (Table 1) differ by less than ~ 10 ka in the Brunhes chron. Furthermore, the astronomically derived age models agree well with radiometric datings (e.g. [7]). The effect of using an untuned timescale for DSDP 607, ODP 659 and ODP 677 on 100 ka envelope estimates has been found to be negligible [11]. The maximum possible bias of the time domain estimates in the Brunhes/Matuyama–Jaramillo interval is ~ 50 ka (midpoint times), and ~ 15 ka (durations), respectively.

4. Discussion: ice–bedrock model simulation

Even if one considers the uncertainties due to the statistical estimations and potential inaccuracies of the timescales of the $\delta^{18}O$ records, one is confronted with the fact that the MPT change in 100 ka amplitude significantly lagged the change in $\delta^{18}O$ mean by ~ 280 ka. Considering the global distribution of the cores and the different habitats of the foraminifera sampled (Table 1) we infer that the MPT was a global phenomenon with a dominating ice volume signal, in accordance with Maasch [4]. The increase of 0.29 ± 0.05‰ in the $\delta^{18}O$ mean corresponds to an ice mass increase of $1.05 \pm 0.20 \times 10^{19}$ kg (using a ratio $\Delta\ \delta^{18}O{:}\Delta$ sea level of 0.1‰:11 ± 1 m, ice density = 917 kg m^{-3}, and ocean area = 3.62×10^{14} m^2). To check possible physical explanations for this delay, for example, bedrock relaxation (see [19]), we simulate our results with an ice–bedrock model [1].

We apply the most simple form of the model ([1]; case I therein) with only two variables: ice mass (of the Northern Hemisphere ice sheets without the Greenland ice sheet) and bedrock depression. The system is driven by Milankovitch forcing (July 65°N insolation; [20]). Calving instabilities are allowed at times of ice sheet retreat and are caused by a bedrock depression which is too high in relation to the existing ice mass. Fulfilment of the latter condition is triggered by an increased insolation. Our estimated increase in mean ice mass across the MPT is prescribed by linearly increasing the model ice accumulation rate (see [1]; eq. 22 therein) from 2.1×10^{15} kg/a (corresponding to an equilibrium ice mass of 2.1×10^{19} kg) at time $T = 942$ ka to 3.15×10^{15} kg/a at $T = 902$ ka. The remaining model parameters ([1]; table 1 and eq. 22 therein) are adjusted such that the MPT increase in mean ice mass causes the bedrock to be depressed further and, hence, the critical calving threshold to be exceeded. In this way pseudo-regular calving cycles with periods between ~ 76 and 100 ka are initiated. (Model parameters: insolation factor = 0.64×10^{14} kg a^{-1}/(W m^{-2}),

undepressed topographic elevation = 543 m, and bedrock response time = 30 ka.)

Fig. 3 shows the simulated ice mass across the MPT. The characteristics of the 100 ka envelopes of the $\delta^{18}O$ time series measured (Fig. 2) — midpoint time 641 ka, abruptness, and amplitude increase of roughly 0.4‰ — are well reproduced by the model. Calving starts at 860 ka; that is, after about (922 ka —860 ka) $\approx 2 \times$ the bedrock response time subsequent to the increase in ice accumulation rate. With the next two calving events (783 ka and 707 ka) a temporal separation is exhibited (77 ka and 76 ka), which is clearly less than 100 ka. With the following peak (618 ka) the $\sim$100 ka cycle starts, resulting in a transition midpoint of $\sim$650 ka for the 100 ka envelope of the modelled ice mass (Fig. 3). The modelled delay between the ice accumulation increase (corresponding to the measured increase in $\delta^{18}O$ mean) and the onset of the $\sim$100 ka cycle is not caused by bedrock relaxation alone. The characteristic timescale of the latter process is clearly smaller than the observed delay. It is the coincidental combination of insolation, existing ice mass, and bedrock depression that causes transitions from non-calving to $\sim$77 ka-calving to $\sim$100 ka-calving in the nonlinear ice–bedrock system. The modelled evolution of the spectral character is in accordance with previous findings [10] on measured $\delta^{18}O$ records. The simulated calving times agree reasonably well with deglaciation peaks of Pleistocene

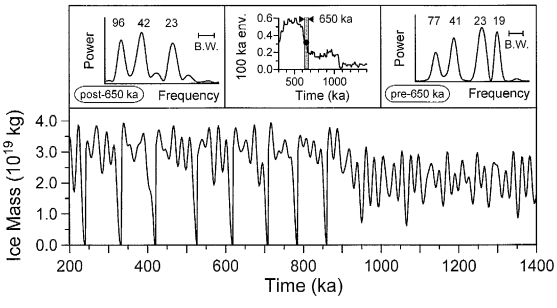

Fig. 3. Simulated Pleistocene ice mass against time, power spectra (periods labelled in ka; B.W. = bandwidth), and 100 ka envelope (re-calculated into ‰ units; transition midpoint marked) of the simulated time series. The spectral peak at 1/77 ka in the pre-650 ka time series results from the first three calving events (see text for details).

$\delta^{18}O$ standard curves (e.g. [21]). The modelled pseudo-periodic character of the $\sim$100 ka cycle (see [5]) has been recently confirmed by Mann and Lees [22]. The simulated glacial–interglacial $\delta^{18}O$ amplitudes (pre-MPT: $\sim$0.6‰; post-MPT: $\sim$1.1‰; using the same conversion factor as above) are about 2/3 of the measured amplitudes.

The MPT is inferred to be a non-synchronous transition in the time and frequency domains. This transition was triggered by a rapid increase in mean ice volume, in accordance with previous work [2], which led to the critical calving threshold being exceeded.

A lowered atmospheric CO_2 content may have contributed to the MPT change in mean ice volume by permitting a higher rate of ice accumulation [1,2]. As has been considered [2], the additional ice could have been stored in the Barents and Kara Sea regions, which were covered by an ice sheet of 3.8×10^{12} m^2 at the Last Glacial Maximum [23]. Using the relation between mass and dimensions of an ice dome ([1], p. 7), our inferred ice mass increase of $1.05 \pm 0.20 \times 10^{19}$ kg corresponds to an increase in ice sheet area of $3.1 \pm 0.7 \times 10^{12}$ m^2. Further support for this location is that it is suited for marine-based ice sheets [2] which are susceptible to calving and ''may account for the changes ... in the spectral character of the ice-volume record'' [5].

5. Conclusions

The Mid-Pleistocene Climate Transition consisted of a $\delta^{18}O$ increase of 0.29 ± 0.05‰ (expanding ice mass and minor temperature effect). This transition in mean was centred at 922 ± 12 ka and had a duration of 40 ± 9 ka. The MPT increase in 100 ka amplitude was abrupt at 641 ± 9 ka. Hence, the onset of the Late Pleistocene $\sim$100 ka cycle significantly lagged the MPT ice mass increase by about 280 ka (Fig. 4).

Using a simple ice–bedrock model this finding can be simulated quantitatively. Due to the increase in mean ice mass the critical calving threshold was exceeded. This led to three calving events which are separated by $\sim$77 ka. Only after $\sim$650 ka was the $\sim$100 ka cycle started. Thus, the delay was a result of the coincidental combination of insolation, ice

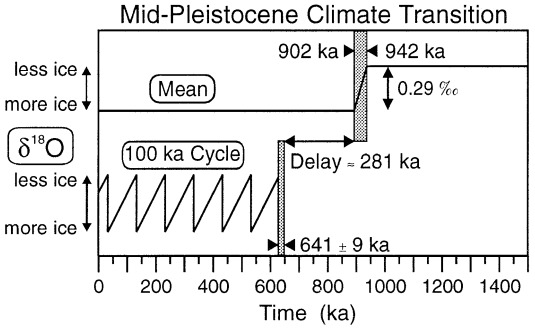

Fig. 4. Schematic view of the Mid-Pleistocene Climate Transition in the time and frequency domains (see text for details).

mass, and bedrock depression. It was not caused by slow bedrock relaxation.

From the MPT $\delta^{18}O$ increase we estimate an increase in ice mass of $1.05 \pm 0.20 \times 10^{19}$ kg. This corresponds to an increase in ice sheet area of $3.1 \pm 0.7 \times 10^{12}$ m^2, thus supporting Berger and Jansen [2] who considered that the additional MPT ice led to the formation of the Barents/Kara ice sheet.

Acknowledgements

We thank A. Berger and an anonymous reviewer for critical comments on the manuscript. Helpful suggestions by P. Grootes and K. Stattegger are appreciated. W.H. Berger, M.K. Yasuda, M.E. Raymo and R. Tiedemann kindly provided their data. MS is supported by the Deutsche Forschungsgemeinschaft within the framework of the SFB 313 at Kiel University. *[AC]*

References

[1] B. Saltzman, M.Y. Verbitsky, Multiple instabilities and modes of glacial rhythmicity in the Plio–Pleistocene: A general theory of late Cenozoic climatic change, Climate Dyn. 9 (1993) 1–15.

[2] W.H. Berger, E. Jansen, Mid-Pleistocene climate shift — the Nansen connection, in: O.M. Johannessen, R.D. Muench, J.E. Overland (Eds.), The Polar Oceans and Their Role in Shaping the Global Environment, Am. Geophys. Union Geophys. Monogr. 85 (1994) 295–311.

[3] W.L. Prell, Oxygen and carbon isotope stratigraphy for the Quaternary of hole 502B: Evidence for two modes of isotopic variability, Init. Rept. DSDP 68 (1982) 455–464.

[4] K.A. Maasch, Statistical detection of the mid-Pleistocene transition, Climate Dyn. 2 (1988) 133–143.

[5] N.G. Pisias, T.C. Moore Jr., The evolution of Pleistocene climate: A time series approach, Earth Planet. Sci. Lett. 52 (1981) 450–458.

[6] W.F. Ruddiman, M.E. Raymo, D.G. Martinson, B.M. Clement, J. Backman, Pleistocene evolution: Northern hemisphere ice sheets and North Atlantic Ocean, Paleoceanography 4 (1989) 353–412.

[7] W.H. Berger, M.K. Yasuda, T. Bickert, G. Wefer, T. Takayama, Quaternary time scale for the Ontong Java Plateau: Milankovitch template for Ocean Drilling Program site 806, Geology 22 (1994) 463–467.

[8] K.-M. Lau, H. Weng, Climate signal detection using wavelet transform: How to make a time series sing, Bull. Am. Meteorol. Soc. 76 (1995) 2391–2402.

[9] J. Park, K.A. Maasch, Plio–Pleistocene time evolution of the 100-kyr cycle in marine paleoclimate records, J. Geophys. Res. 98 (1993) 447–461.

[10] E.W. Bolton, K.A. Maasch, J.M. Lilly, A wavelet analysis of Plio–Pleistocene climate indicators: A new view of periodicity evolution, Geophys. Res. Lett. 22 (1995) 2753–2756.

[11] M. Mudelsee, Entwicklung neuer statistischer Analysemethoden für Zeitreihen mariner, stabiler Isotopen: die Evolution des globalen Plio-/Pleistozänen Klimas, Ph.D. Thesis, Univ. Kiel, 1995.

[12] M. Schulz, SPECTRUM und ENVELOPE: Computerprogramme zur Spektralanalyse nicht äquidistanter paläoklimatischer Zeitreihen, Ber. Sonderforschungsber. Univ. Kiel 313, 65 (1996) 131 pp.

[13] S. Ferraz-Mello, Estimation of periods from unequally spaced observations, Astron. J. 86 (1981) 619–624.

[14] N.J. Shackleton, M.A. Hall, Oxygen and carbon isotope stratigraphy of Deep Sea Drilling Project hole 552A: Plio–Pleistocene glacial history, Init. Rept. DSDP 81 (1984) 599–609.

[15] R. Tiedemann, M. Sarnthein, N.J. Shackleton, Astronomic timescale for the Pliocene Atlantic $\delta^{18}O$ and dust flux records of Ocean Drilling Program site 659, Paleoceanography 9 (1994) 619–638.

[16] N.J. Shackleton, M.A. Hall, Stable isotope history of the Pleistocene at ODP site 677, Proc. ODP Sci. Results 111 (1989) 295–316.

[17] N.J. Shackleton, A.L. Berger, W.R. Peltier, An alternative astronomical calibration of the lower Pleistocene timescale based on ODP Site 677, Trans. R. Soc. Edinburg Earth Sci. 81 (1990) 251–261.

[18] W.H. Berger, T. Bickert, H. Schmidt, G. Wefer, Quaternary oxygen isotope record of pelagic foraminifers: site 806, Ontong Java Plateau, Proc. ODP, Sci. Results 130 (1993) 381–395.

[19] C. Emiliani, J. Geiss, On glaciations and their causes, Geol. Rundsch. 46 (1957) 576–601.

[20] A.L. Berger, M.F. Loutre, Insolation values for the climate of the last 10 million years, Quat. Sci. Rev. 10 (1991) 297–317.

[21] F.C. Bassinot, L.D. Labeyrie, E. Vincent, X. Quidelleur, N.J. Shackleton, Y. Lancelot, The astronomical theory of climate and the age of the Brunhes–Matuyama magnetic reversal, Earth Planet. Sci. Lett. 126 (1994) 91–108.

[22] M.E. Mann, J.M. Lees, Robust estimation of background noise and signal detection in climatic time series, Clim. Change 33 (1996) 409–445.

[23] D.D. Kvasov, A.I. Blazhchishin, The key to sources of the Pliocene and Pleistocene glaciation is at the bottom of the Barents Sea, Nature 273 (1978) 138–140.